Supporting Information

High Lithium Ion Diffusion SiO_2@MoS_2 Core-Shell Nanocomposite Layers as Triple Polysulfide Shield for High Performance Lithium-Sulfur Batteries

Jingyi Wu, Na You, Xiongwei Li, Honagxia Zeng, Shuai Li, Zhigang Xue, Yunsheng Ye, Xiaolin Xie**

Li^+ diffusion coefficient (D_{Li^+})

After cycling at 0.1 C for 4 cycles for activation, the CV curves at the fourth scan were taken for conducting D_{Li^+} analysis. D_{Li^+} was examined by the Randles-Sevcik equation:

$$I_p = 2.69 \times 10^5 n^{3/2} A D_{Li^+}^{1/2} C_{Li^+} v^{1/2}$$

where I_p is the peak current, n is the number of electrons transferred in the reaction (n=2 for Li-S batteries), A is the electrode area, D_{Li^+} is the Li^+ diffusion coefficient, C_{Li^+} is the Li^+ concentration, and v refers to the scan rate. I_p was normalized by the capacity fade.

Li^+ conductivity

To estimate the influence of the interlayer on the ionic conductivity, the functional materials was tape cast on the surface of Celgard separator with a coating thickness of ~10 μm. The ionic conductivity of the coated separator was measured by EIS method and calculated using the equation $\sigma = \frac{L}{R_b S}$, where L and S are the thickness and area of the separator/or modified separator, respectively, and R_b is the bulk Ohmic resistance of the electrolyte.

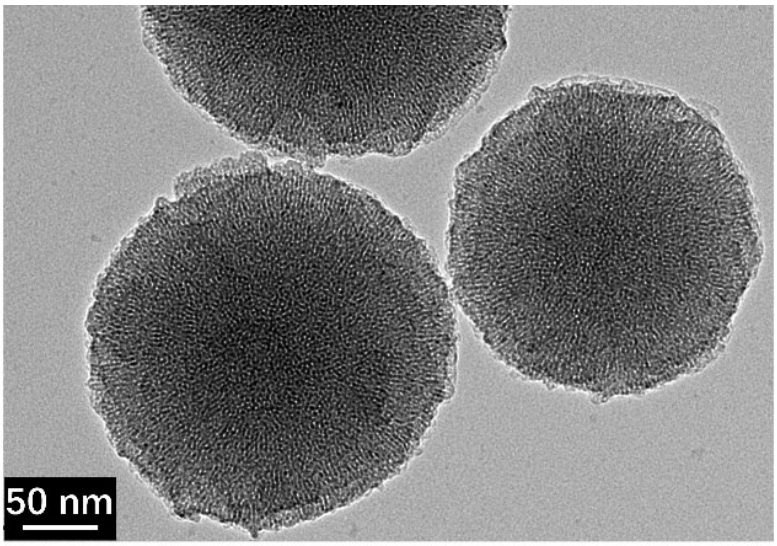

Fig. S1 HRTEM image of the mesoporous SiO_2 nanospheres.

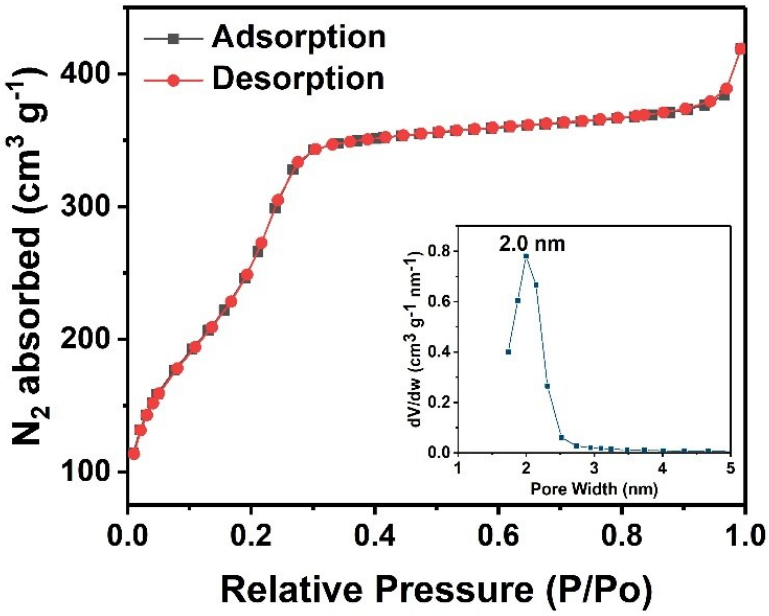

Fig. S2 N_2 adsorption-desorption isotherms of the mesoporous SiO_2 nanospheres.

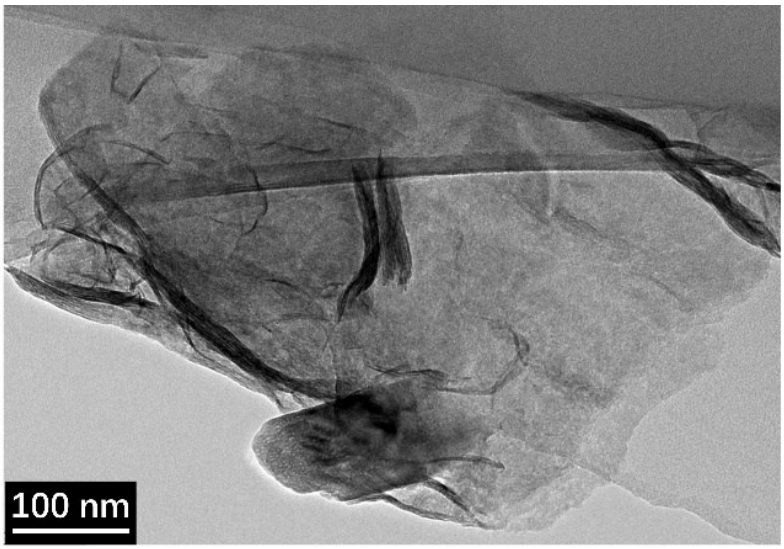

Fig. S3 HRTEM image of the exfoliated MoS_2.

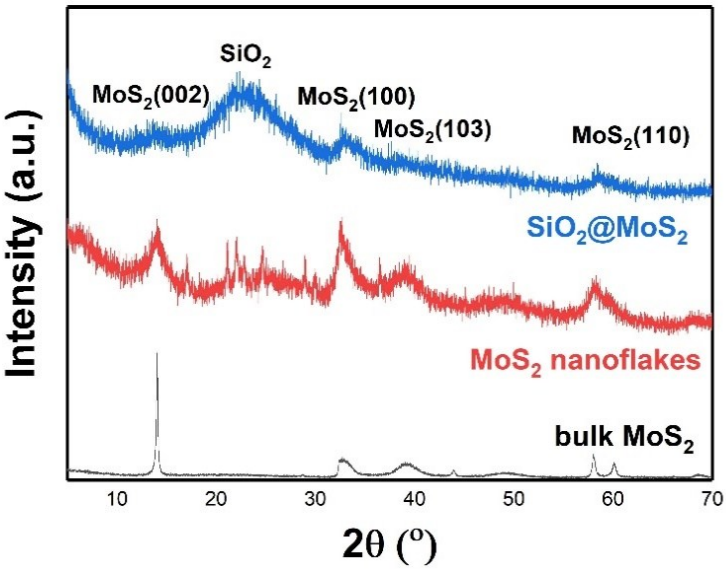

Fig. S4 XRD patterns of SiO_2@MoS_2, MoS_2 nanoflakes and bulk MoS_2.

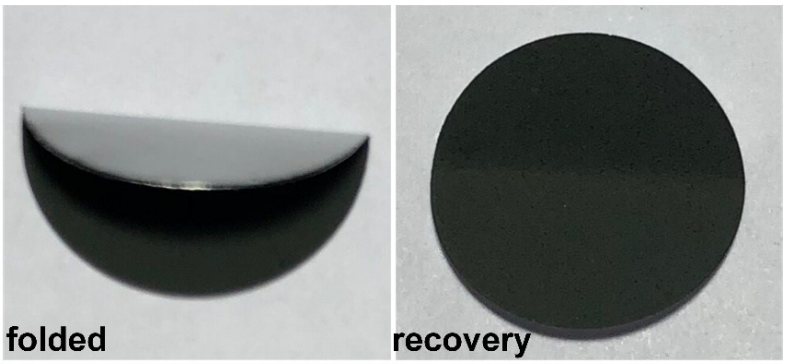

Fig. S5 Folded-recovery test of the SiO_2@MoS_2 interlayer coated cathode, showing excellent adhesion.

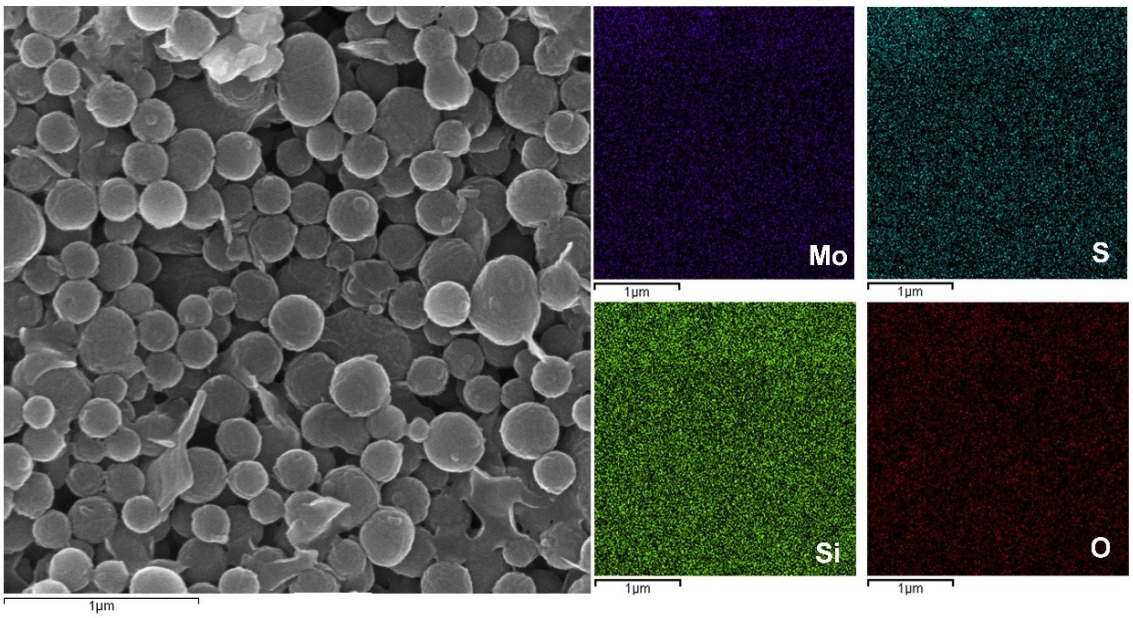

Fig. S6 SEM and the corresponding elemental maps of the surface of the SiO_2@MoS_2 coated cathode.

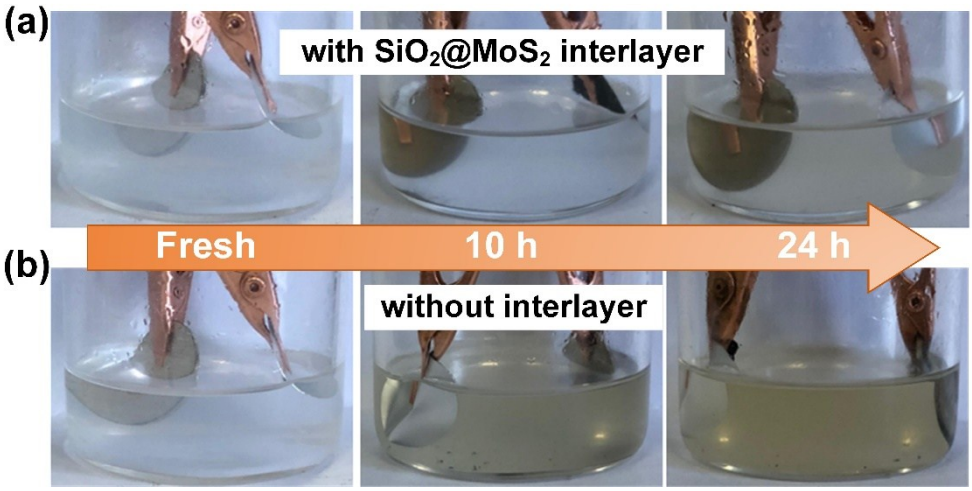

Fig. S7 Visual examination of PS entrapment at different cycle times of Li-S batteries with (a) the SiO_2@MoS_2 interlayer coated cathode and (b) the sulfur cathode without an interlayer, both at current rate of 1 C.

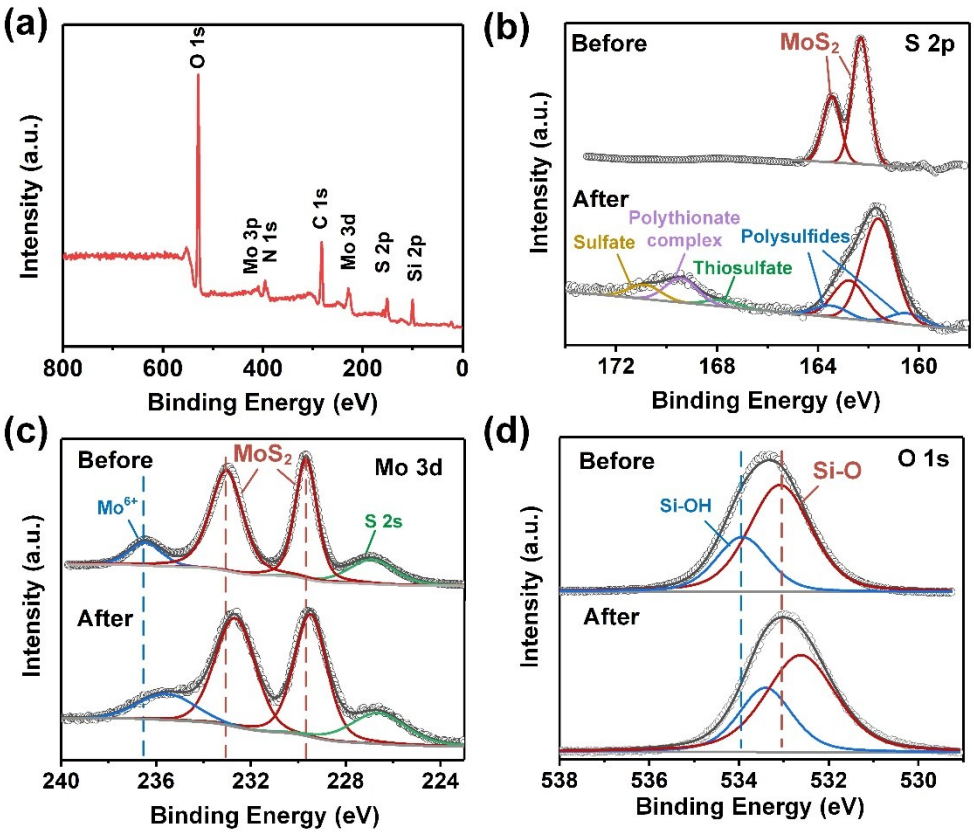

Fig. S8 (a) XPS survey spectra of SiO_2@MoS_2. (b) S 2p, (c) Mo 3d and (d) O 1s XPS spectra of SiO_2@MoS_2 nanocomposites before and after PS adsorption.

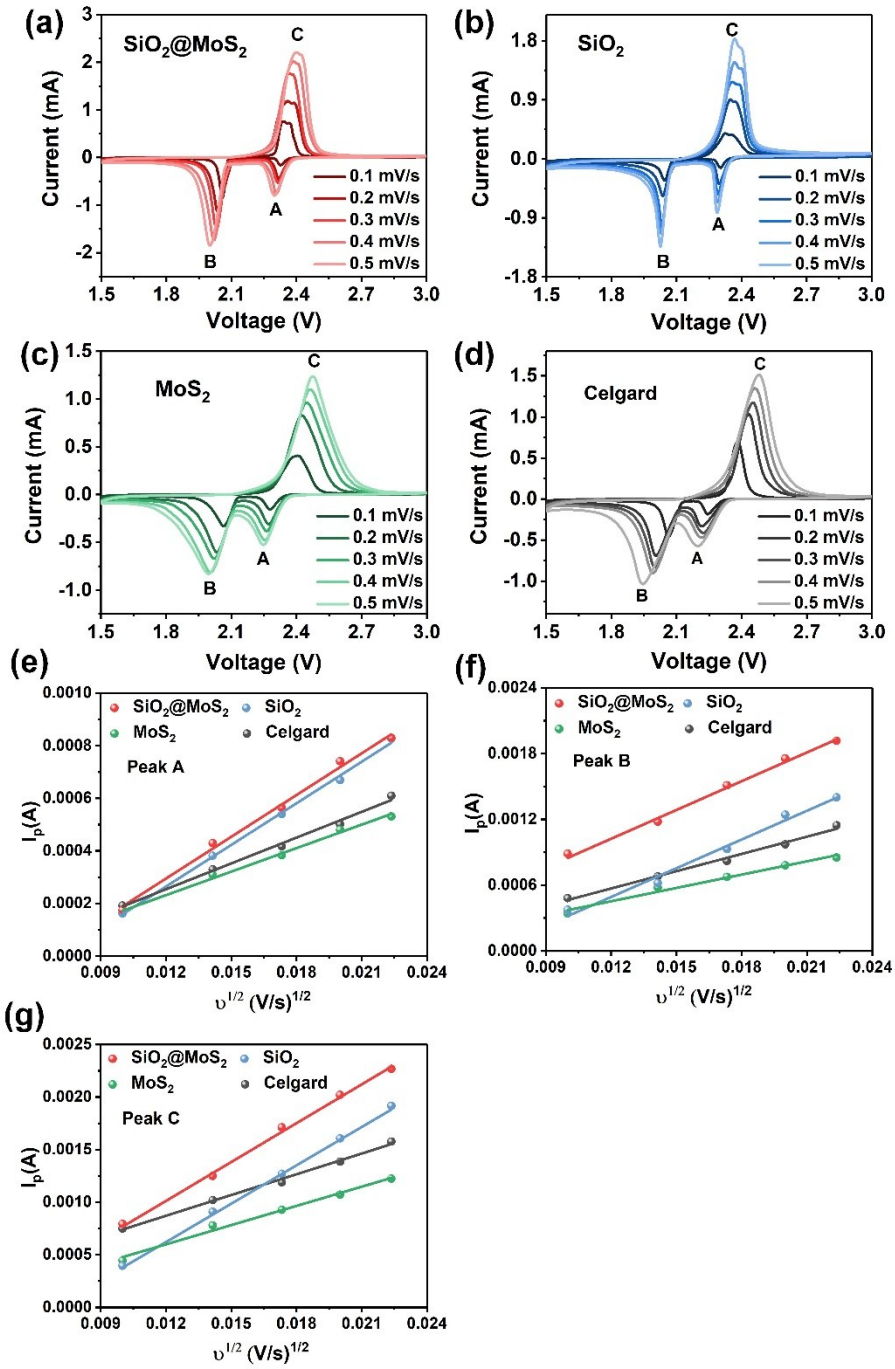

Fig. S9 CV curves at various scan rates of the cells with (a) the SiO_2@MoS_2, (b) the mesoporous SiO_2, (c) the MoS_2 nanoflake interlayers and (d) without any interlayer. Plots of the CV peak current (I_p) versus the square root of the scan rate ($v^{1/2}$) at: (e) the cathodic peak at around 2.35 C (peak A), (f) the cathodic peak at around 2.05 V (peak B) and (g) the anodic peak (peak C).

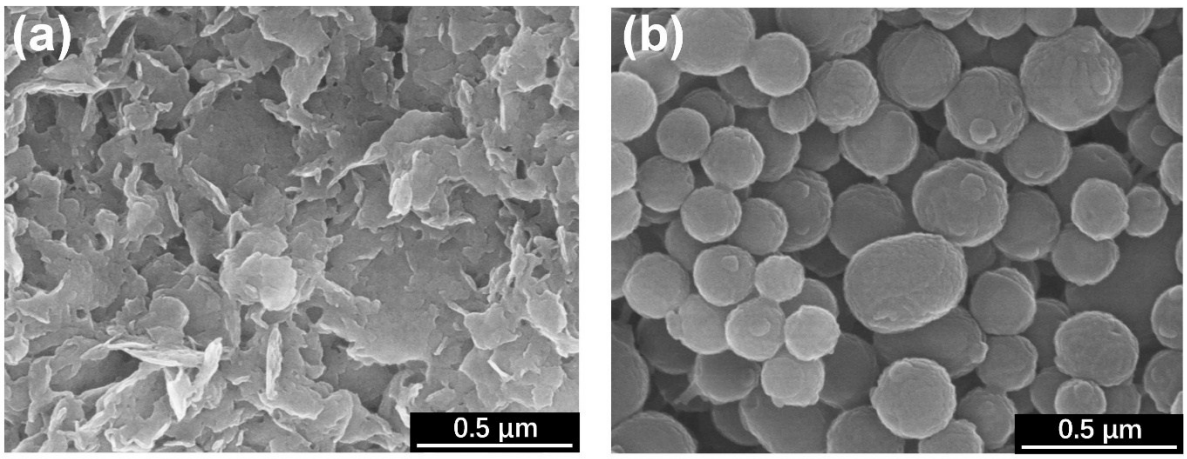

Fig. S10 SEM images of the MoS_2 nanoflake interlayer (a) and the mesoporous SiO_2 interlayer (b).

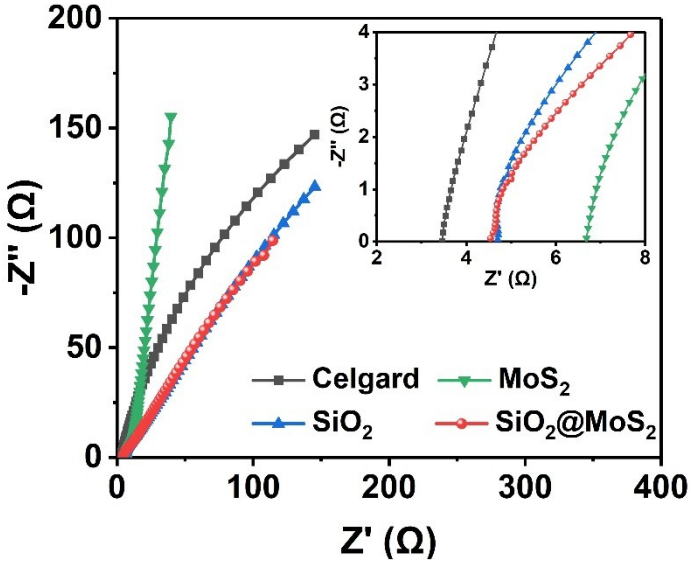

	Celgard	MoS_2	SiO_2	SiO_2@MoS_2
Li^+ conductivity (mS cm^{-1})	0.51	0.40	0.65	0.66

Fig. S11 EIS curves of different interlayer coated separators and the corresponding ionic conductivities.

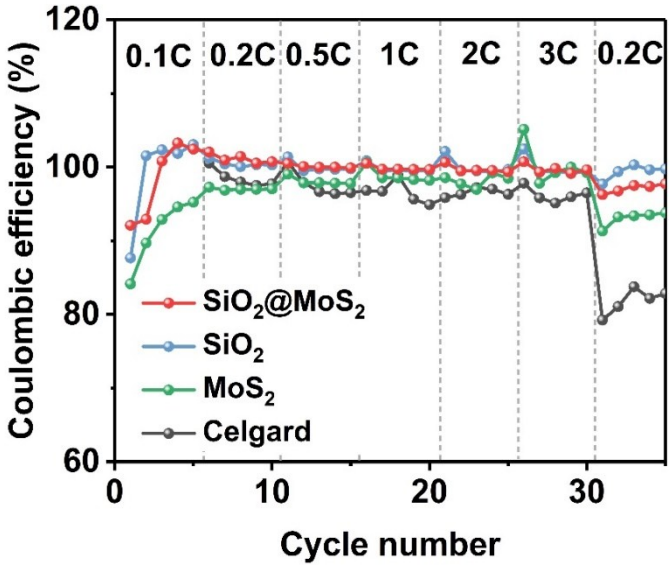

Fig. S12 Coulombic efficiencies of cells with different configurations during the rate performance.

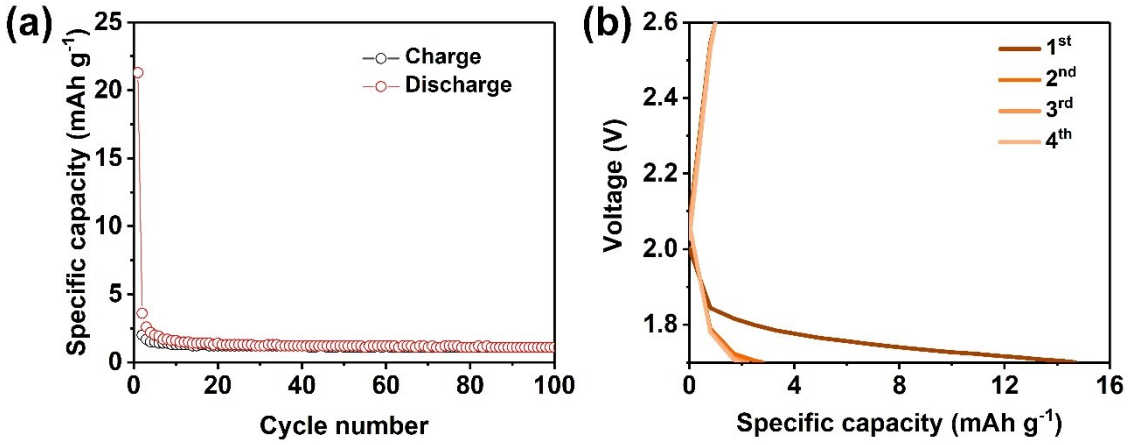

Fig. S13 (a) Cycling performance at 1 C and (b) the corresponding charge-discharge profiles of MoS_2 naonsheets anode as a typical Li-S battery in a voltage window of 1.7-2.6 V vs Li^+|Li. MoS_2 anode was prepared by mixing MoS_2 nanosheets and PVDF (weight ratio of 9:1) in NMP and then cast the slurry on Al foil..

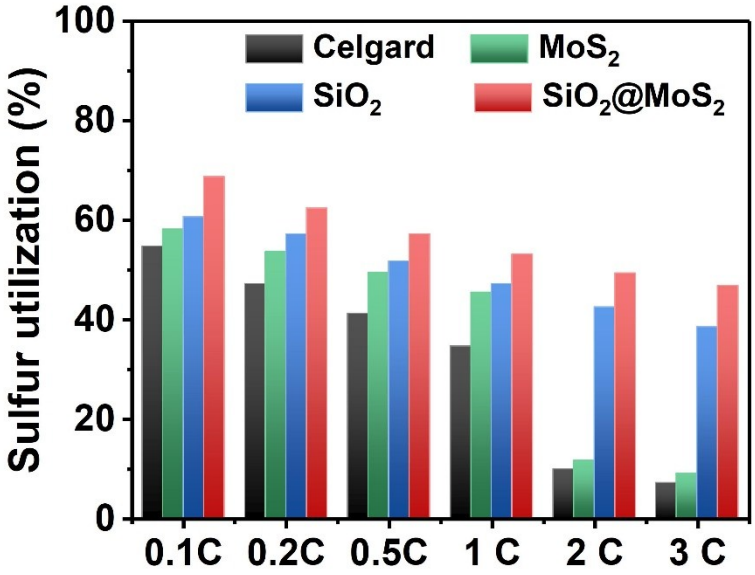

Fig. S14 The sulfur utilization rate of different batteries at various rates.

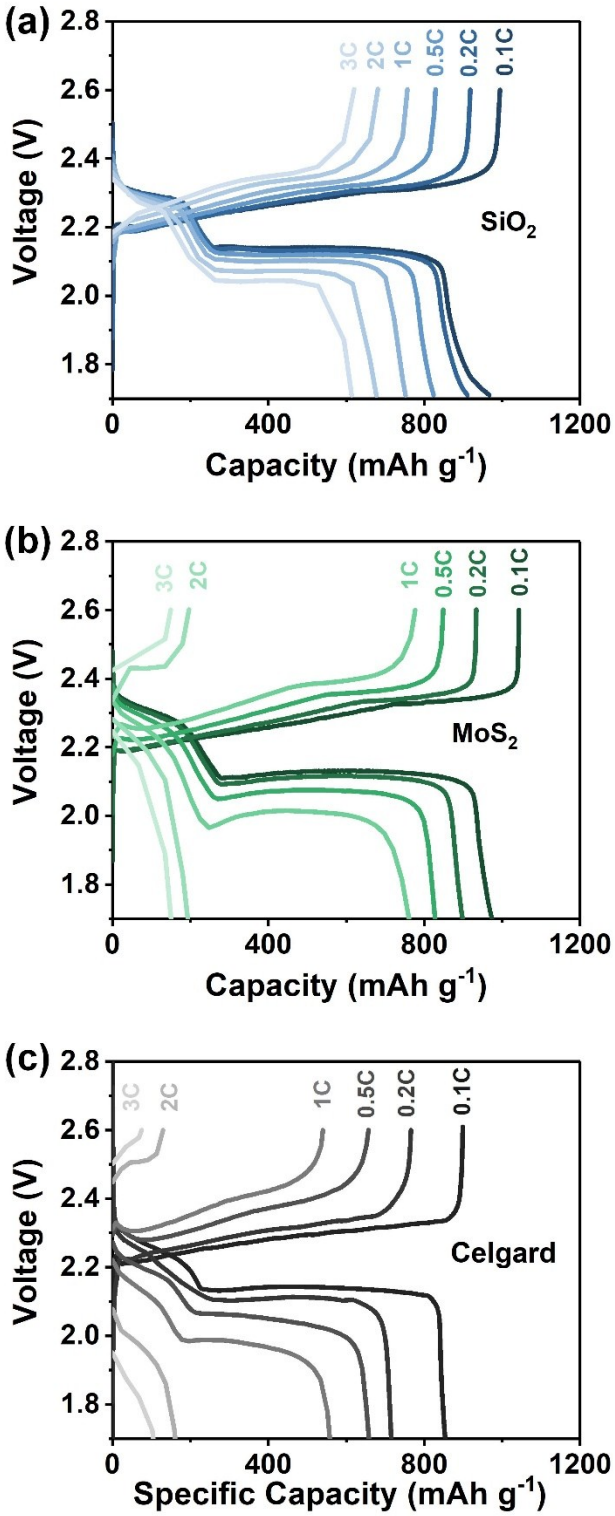

Fig. S15 Galvanostatic charge-discharge profiles at various current rates of cells with (a) the mesoporous SiO_2, (b) the MoS_2 nanoflake interlayers and (c) without any interlayer.

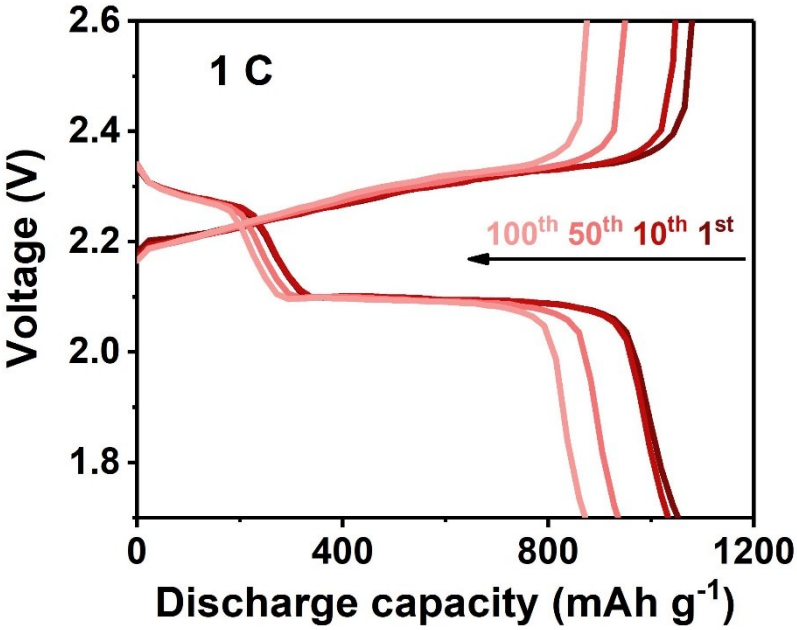

Fig. S16 Galvanostatic charge-discharge curves of the cell with the SiO_2@MoS_2 interlayer at 1 C.

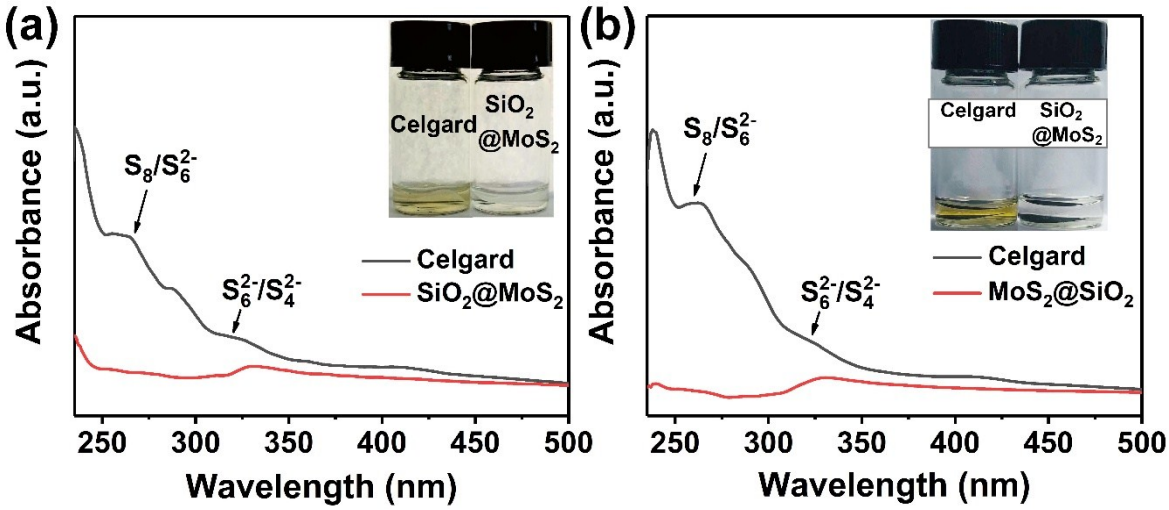

Fig. S17 UV-Vis spectra and photographs (inset) of the cycled (a) separators and (b) cathodes in THF.

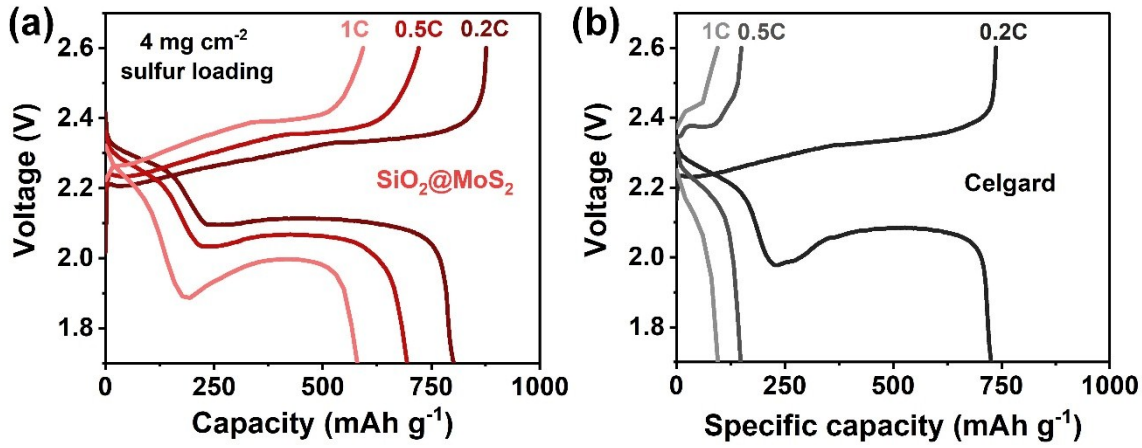

Fig. S18 Galvanostatic charge-discharge curves of cells with (a) the SiO_2@MoS_2 interlayer and (b) without any interlayer at a raised sulfur loading of 4.0 mg cm^{-2}.

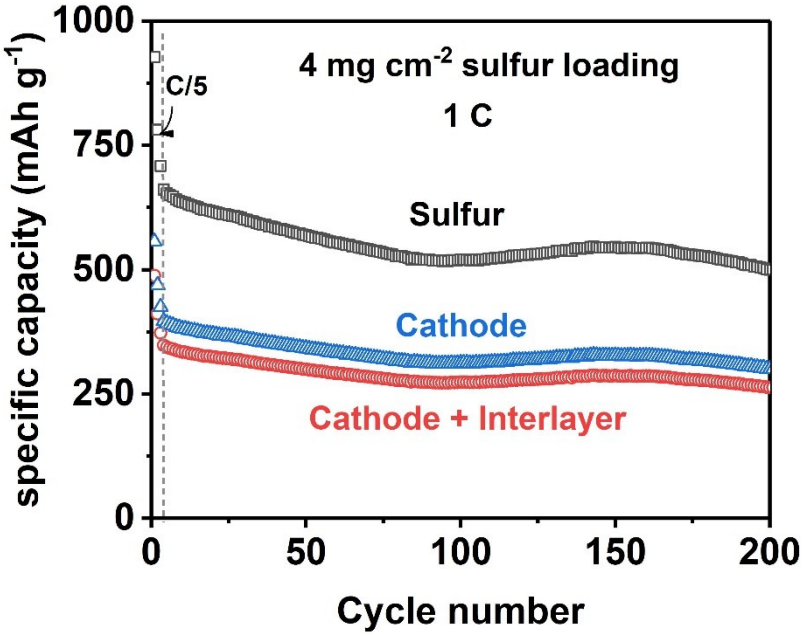

Fig. S19 Rate performance at a sulfur loading of 4.0 mg cm^{-2}. Specific capacies are calculated based on the mass of sulfur (black), total mass of the cathode (blue) and the total mass of the cathode and the SiO_2@MoS_2 interlayer (red).

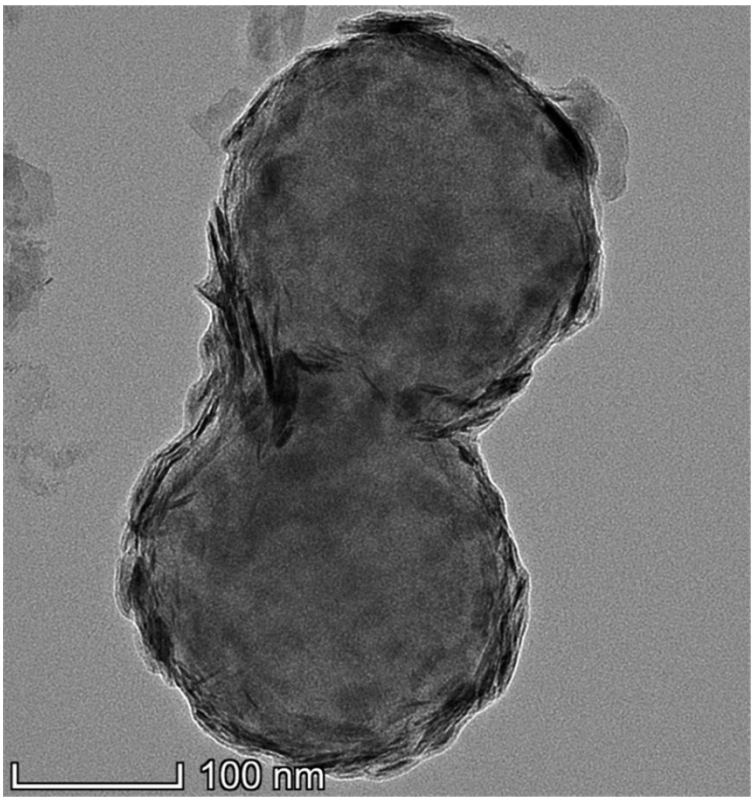

Fig. S20 TEM image of SiO_2@WS_2.

Table S1 Li^+ diffusion coefficients of cells with different configurations calculated from the Randles-Sevcik equation after adjusting for capacity fade.

Sample	**D_{Li^+} at peak A ($cm^2\ s^{-1}$)**	**D_{Li^+} at peak B ($cm^2\ s^{-1}$)**	**D_{Li^+} at peak C ($cm^2\ s^{-1}$)**
SiO_2@MoS_2	1.30×10^{-8}	3.56×10^{-8}	7.04×10^{-8}
SiO_2	1.29×10^{-8}	3.54×10^{-8}	6.85×10^{-8}
MoS_2	4.12×10^{-9}	7.63×10^{-9}	1.72×10^{-8}
Celgard	4.97×10^{-9}	1.18×10^{-8}	2.01×10^{-8}

Table S2. Summary of the impedance parameters of cells with different configurations.

Parameters	Celgard	MoS_2	SiO_2	SiO_2@MoS_2
R_o (Ω)	7.5	5.1	5.7	4.3
R_{sf} (Ω)	101.5	25.7	40.5	7.0
R_{ct} (Ω)	60.3	33.5	11.1	3.1

Table S3 The electrochemical performance comparison of Li-S batteries with MoS_2-related interlayers in recent publications.

Interlayer	Nanocomposite fabrication method	Cathode	Rate (C)	Cycle life	Capacity decay (%)	Year[ref]
SiO_2@MoS_2	Self-assembly	Pure sulfur	2	2500	0.028	This work
MoS_2/rGO	Hydrothermal method	Pure sulfur	1	500	0.116	2018[1]
MoS_2/CNT	Vacuum filtration	Pure sulfur	1	500	0.061	2018[2]
MoS_2/CNT	Layer-by-layer filtration	S/CNT composites	0.5	500	-	2017[3]
MoS_2	-	Pure sulfur	0.5	600	0.08	2017[4]

Table S4 Comparison of Li-S batteries using prisine sulfur cathodes and various interlayers in recent publications.

Interlayer	Interlayer thickness (μm)	S loading (mg cm^{-2})	S content (%)	S content[a] (%)	Electrolyte volume (μL/mg S)	Capacity fading (% per cycle)	Rate performance (mAh g^{-1})	Year[Ref]
SiO_2@MoS_2	3	1.2, 4.0 (high S)	60	43, 54	15	0.028 (2500th)	783 (3 C)	This work
Sb_2S_3/CNT	10	1.0	65	51	ca. 44[b]	0.049 (1000th)	530 (2 C)	2018[5]
Laponite/CB	3.5	1.0-1.2	70	48	ca. 44[b]	0.028 (500th)	758 (2 C)	2018[6]
MWCNT/NCQD	>20[c]	1.4, 3.0 (high S)	60	56, 58	ca. 51[b]	0.05 (1000th)	667 (3 C)	2018[7]
Mesoporous SiO_2	20	0.75	70	62	-	0.057 (300th)	501 (1 C)	2018[8]
LiF/GO	-	1.3, 2.6 (high S)	80	73, 76	-	0.043 (400th)	524 (3 C)	2018[9]
Niobium Carbide	10	1.5, 4.0 (high S)	60	44, 53	25	0.037 (1500th)	730 (5 C)	2018[10]
Indium Nitride	6.5	1.5	80	69	20	0.015 (1000th)	415 (5 C)	2018[11]
MoP_2/CNT	>20[c]	1.2, 2.8 (high S)	50	44, 47	-	0.025 (500th)	360 (5 C)	2018[12]
MoS_2/rGO	8	1.8-2.0	70	64	ca. 23[b]	0.116 (500th)	615 (2 C)	2018[1]
MoS_2/CNT	2	1.4	50	46	25	0.061 (500th)	784 (10 C)	2018[2]
MoS_2 nanosheets	0.35	-	60	-	65 μL per cell	0.083 (600th)	550 (1 C)	2017[4]
CNT@TiO_2	12	1.7, 3 (high S)	60	48, 53	-	0.056 (1000th)	740 (2 C)	2017[13]
Co/Co_3O_4/TiO_2/N-doped porous C	>20[c]	1.5	60	-	-	0.147 (100th)	651 (1 C)	2017[14]

BN-carbon	13	2.1	60	-	-	0.09 (250th)	702 (4 C)	2017[15]
CNF@δ-MnO2	2	2.1, 4.1 (high S)	80	-	ca. 23[b]	0.13 (200th)	554 (2 C)	2017[16]
V_2O_5/CNF	>20[c]	2.0	70	52	-	0.03 (1000th)	709 (5 C)	2017[17]
Graphene/chitosan	22.5	1.6-2.0	75	71	ca. 18[b]	0.021 (3000th)	750 (2 C)	2017[18]
Acidized CNT	>20[c]	1.0	70	-	-	0.1 (400th)	660 (2 C)	2017[19]
CNT	>20[c]	1.0	70	-	-	0.66 (100th)	466 (2.5 C)	2017[20]
SRGO	10	1.3, 5 (high S)	60	51, 59	-	0.15 (250th)	471 (4 C)	2017[21]
LTO/graphene	35	1.0-1.2	60	50	-	0.03 (500th)	709 (2 C)	2016[22]
GO	-	1.0-1.5	63	59	-	0.23 (100th)	ca. 600 (2 C)	2015[23]
Activated CNF	25	2.1-2.3	70	63	ca. 18[b]	0.13 (200th)	-	2015[24]

[a] S content including the weight of the interlayer. [b] calculated based on a cathode disk 12 mm in diameter. [c] free-standing interlayers usually with thickness > 20 μm. "-" means data not available.

References

1. L. Tan, X. Li, Z. Wang, H. Guo and J. Wang, *ACS Applied Materials & Interfaces*, 2018, **10**, 3707-3713.
2. L. Yan, N. Luo, W. Kong, S. Luo, H. Wu, K. Jiang, Q. Li, S. Fan, W. Duan and J. Wang, *Journal of Power Sources*, 2018, **389**, 169-177.
3. Y. C. Jeong, J. H. Kim, S. H. Kwon, J. Y. Oh, J. Park, Y. Jung, S. G. Lee, S. J. Yang and C. R. Park, *Journal of Materials Chemistry A*, 2017, **5**, 23909-23918.
4. Z. A. Ghazi, X. He, A. M. Khattak, N. A. Khan, B. Liang, A. Iqbal, J. Wang, H. Sin, L. Li and Z. Tang, *Advanced Materials*, 2017, **29**, 1606817.

5. S. Yao, J. Cui, J.-Q. Huang, Z. Lu, Y. Deng, W. G. Chong, J. Wu, M. Ihsan Ul Haq, F. Ciucci and J.-K. Kim, *Advanced Energy Materials*, 2018, **8**, 1800710.

6. Y. Yang and J. Zhang, *Advanced Energy Materials*, 2018, **8**, 1801778.

7. Y. Pang, J. Wei, Y. Wang and Y. Xia, *Advanced Energy Materials*, 2018, **28**, 1702288.

8. N. Zhang, B. Li, S. Li and S. Yang, *Advanced Energy Materials*, 2018, **8,** 1703124.

9. X. Ni, T. Qian, X. Liu, N. Xu, J. Liu and C. Yan, *Advanced Functional Materials*, 2018, **28**, 1706513.

10. W. Cai, G. Li, K. Zhang, G. Xiao, C. Wang, K. Ye, Z. Chen, Y. Zhu and Y. Qian, *Advanced Functional Materials*, 2018, **28**, 1704865.

11. L. Zhang, X. Chen, F. Wan, Z. Niu, Y. Wang, Q. Zhang and J. Chen, *ACS Nano*, 2018, **12**, 9578-9586.

12. Y. Luo, N. Luo, W. Kong, H. Wu, K. Wang, S. Fan, W. Duan and J. Wang, *Small*, 2018, **14**, 1702853

13. L. Yang, G. Li, X. Jiang, T. Zhang, H. Lin and J. Y. Lee, *Journal of Materials Chemistry A*, 2017, **5**, 12506-12512.

14. C.-Y. Fan, S.-Y. Liu, H.-H. Li, Y.-H. Shi, H.-C. Wang, H.-F. Wang, H.-Z. Sun, X.-L. Wu and J.-P. Zhang, *Journal of Materials Chemistry A*, 2017, **5**, 11255-11262.

15. P. J. H. Kim, J. Seo, K. Fu, J. Choi, Z. Liu, J. Kwon, L. Hu and U. Paik, *NPG Asia Materials*, 2017, **9**, 375.

16. Y. Lai, P. Wang, F. Qin, M. Xu, J. Li, K. Zhang and Z. Zhang, *Energy Storage Materials*, 2017, **9**, 179-187.

17. M. Liu, Q. Li, X. Qin, G. Liang, W. Han, D. Zhou, Y. B. He, B. Li and F. Kang, *Small*, 2017, **13**, 1602539.

18. S. A. Abbas, J. Ding, S. H. Wu, J. Fang, K. M. Boopathi, A. Mohapatra, L. W. Lee, P. C. Wang, C. C. Chang and C. W. Chu, *ACS Nano*, 2017, **11**, 12436-12445.

19. G. Xu, A. Kushima, J. Yuan, H. Dou, W. Xue, X. Zhang, X. Yan and J. Li, *Energy &*

Environmental Science, 2017, **10**, 2544-2551.

20. M. Li, W. Wahyudi, P. Kumar, F. Wu, X. Yang, H. Li, L. J. Li and J. Ming, *ACS Applied Materials & Interfaces*, 2017, **9**, 8047-8054.

21. Y. Lu, S. Gu, J. Guo, K. Rui, C. Chen, S. Zhang, J. Jin, J. Yang and Z. Wen, *ACS Applied Materials & Interfaces*, 2017, **9**, 14878-14888.

22. Y. Zhao, M. Liu, W. Lv, Y.-B. He, C. Wang, Q. Yun, B. Li, F. Kang and Q.-H. Yang, *Nano Energy*, 2016, **30**, 1-8.

23. J.-Q. Huang, T.-Z. Zhuang, Q. Zhang, H.-J. Peng, C.-M. Chen and F. Wei, *ACS Nano*, 2015, **9**, 3002-3011.

24. S.-H. Chung, P. Han, R. Singhal, V. Kalra and A. Manthiram, *Advanced Energy Materials*, 2015, **5**, 1500738.